MEASUREMENTS OF X-RAY SPECTRA ON ECR-II*

B. P. Cluggish#, I. N. Bogatu, L. Zhao, J.S. Kim, FAR-TECH, Inc., San Diego, CA 92121 USA.
R. C. Vondrasek, R.C. Pardo, R. H. Scott, ANL, Argonne, IL 60439

Abstract

FAR-TECH, Inc. has been developing an inexpensive and robust X-ray spectral diagnostic for monitoring electron cyclotron resonance ion sources (ECRIS). To this end, FAR-TECH, Inc. has recently performed extensive measurements of X-ray emission from the ECR-II device in the ATLAS facility at Argonne National Laboratory. We find that both the intensity and the shape of the observed spectra are highly correlated with the charge state distribution (CSD) of ions extracted from the ECR-II plasma as measured by a Faraday cup (FC).

INTRODUCTION

X-ray measurements provide much useful information about ECRIS plasmas. The intensity, width, and energy shift of the *K* and *L* lines provide information about the species present in the plasma and their charge states. The bremsstrahlung continuum provides information about the electron distribution function (EDF). The EDF determines both the ionization rates as well as the particle confinement time, thus determining the CSD. This information can be of great use in improving ECRIS modeling codes. In addition, X-ray measurements are non-invasive and can be made without taking the beam offline. However, many X-ray detectors, such as crystal spectrometers [1] or CCD cameras [2] are expensive (~$100K) and/or difficult to use and maintain. In addition, many detectors have limited energy range (< 20 keV) [2], which is insufficient for measuring the bremsstrahlung spectra, where photon energies can be over 100 keV. Therefore, FAR-TECH, Inc. has been developing an inexpensive, robust X-ray diagnostic tool for ECRIS plasmas.

EXPERIMENTAL SETUP

The X-ray measurements described here were performed using an Amptek XR-100T-CdTe detector [3]. The CdTe diode has a detection efficiency of over 20% from 2 to 200 keV and an energy resolution of 600 eV at 60 keV. The detector was controlled using an Amptek PX4 digital pulse processor. The detector and controller together cost only $10K.

The detector was installed on the ECR-II device [4] at the ATLAS facility at Argonne National Laboratory. The detector was installed inside the vacuum chamber through a side port so as to have a view across the plasma transverse to the axis of the device, as shown in Figure 1. The port is located at the midplane of the plasma, where the X-ray detector can view the plasma through apertures between the hexapole magnets. Considerable care was taken ensure that only X-rays generated by collisions in the plasma would be detected, and not X-rays generated by electron collisions with the walls of the device. Lead shielding and two, 2 mm thick, tungsten collimator plates separated by a tungsten spacer blocked all line-of-sight X-rays except those passing through the collimator holes. The holes in the collimator plates (100 μm and 200 μm) are small enough that the solid angle viewed by the detector passes through apertures on either side of the plasma chamber without intersecting it. Thus, only X-rays generated in the plasma pass through the collimator holes.

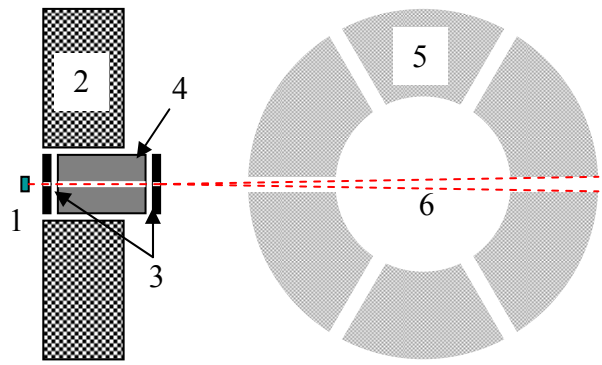

Figure 1: Experimental setup of the X-ray diagnostic. (Not to scale.) Device axis is perpendicular to the page. All components shown are in vacuum. (1) CdTe detector (2) Lead shielding (3) Collimator plates (4) Tungsten spacer (5) Plasma chamber (6) Viewing solid angle

The X-ray measurements presented here were performed on argon plasmas. Unless otherwise stated, the operating parameters were RF frequency ω_{RF} = 14 GHz, minimum magnetic field B_{min} = 3080 G, argon pressure p = 8 x 10^{-8} torr, and RF power P_{RF} = 300 W. The charge state distribution (CSD) of extracted ions was measured with an analyzing magnet and Faraday cup. The RF frequency at 14 GHz is resonant with the electron cyclotron motion at a magnetic field of B_{ECR} = 5000 G, so B_{min}/B_{ECR} = 0.62.

Typical acquisition times for X-ray spectra were 20 minutes for ~10^6 counts. Figure 2 shows a typical raw spectrum acquired on ECR-II. Characteristic K_α and K_β ($K_{\alpha/\beta}$) lines for different species visible to the detector are easily seen. Lead is in the shielding, tungsten is in the collimator, and CdTe is in the detector itself. The argon $K_{\alpha/\beta}$ line disappears if a different working gas is used, which shows that it comes from the plasma and is not an artifact of the detector.

Most of the X-ray counts come from the bremsstrahlung continuum. Our measurements showed a broad peak in the continuum around 120 keV, similar to

*This research was performed under a U.S. DOE SBIR grant and the Office of Nuclear Physics under contract # DE-AC02-06CH11357.
#cluggish@far-tech.com

that observed by other researchers [5,6]. It is unlikely that this broad peak is due to bremsstrahlung alone, since theory predicts that the bremsstrahlung spectrum should monotonically decrease with energy. Instead, we attribute this peak to X-rays that circumvent the lead and tungsten shielding by diffusing through the copper magnets and steel vacuum chamber by Compton scattering. Only X-rays with energies above 100 keV or so can do this; lower energy X-rays are absorbed, resulting in the observed broad peak.

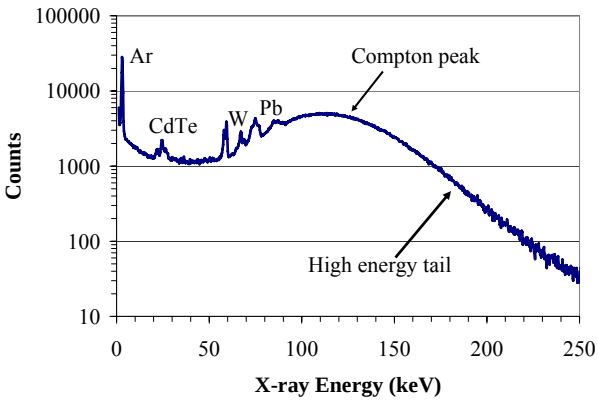

Figure 2: Typical X-ray spectrum, with $K_{\alpha/\beta}$ lines of lead (Pb), tungsten (W), argon (Ar) and CdTe labeled.

Multiplying the raw counts, $C(E)$, by X-ray energy E and dividing by the detection efficiency, $\eta(E)$ [7], and the acquisition time τ gives the X-ray power spectrum:

$$\frac{dP_{XR}}{dE} = \frac{C(E)}{\tau\eta(E)}E$$

The contamination of the spectra by the Compton scattering peak prevented us from determining the EDF from the bremsstrahlung spectrum. However, we can determine an effective temperature of the tail of the EDF, T_{eff}, by fitting a line to logarithm of the exponentially decreasing high energy tail of the power spectrum:

$$\frac{dP_{XR}}{dE} \sim \exp\left(-\frac{E}{T_{eff}}\right)$$

This effective temperature is a relative measurement of the distribution of high energy electrons, but not a direct measurement of the EDF. Another useful quantity is the total measured X-ray power, obtained by integrating the power spectrum over energy:

$$P_{XR} = \int \frac{dP_{XR}}{dE}dE$$

The range of integration can be the whole spectrum to give the total X-ray power or just over the width of a $K_{\alpha/\beta}$ line to give the power in that line.

EXPERIMENTAL RESULTS

The X-ray signal from the plasma was found to depend strongly on the plasma parameters, often more strongly than the CSD. In general, an increase in intensity or effective temperature was accompanied by a shift in the CSD towards higher charge states.

The dependence of X-ray intensity on the pressure of the argon working gas is shown in Figure 3. The plot shows that the intensity of the bremsstrahlung decreases with increasing argon pressure even as the intensity of the argon $K_{\alpha/\beta}$ line increases. This is probably because while increasing the argon pressure reduces the number of high energy electrons, there are still plenty of electrons left with sufficient energy (~3 keV) to ionize the K shell of argon.

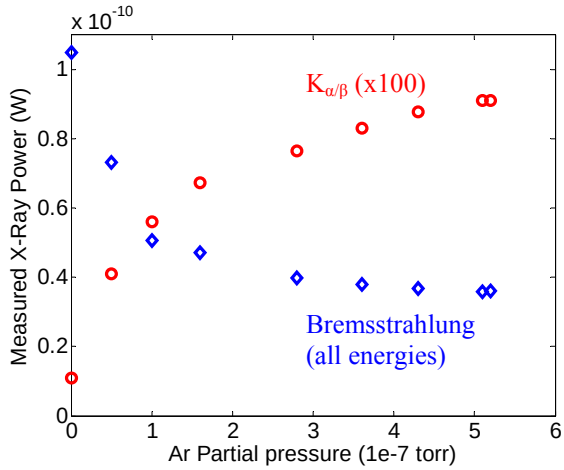

Figure 3: The measured X-ray power, P_{XR}, over all energies (diamonds) and in the argon $K_{\alpha/\beta}$ line (circles) vs. the argon pressure. The $K_{\alpha/\beta}$ data has been multiplied by 100. Note that at "zero" pressure there was still a small but non-zero argon flow.

We have also studied the effect of two-frequency heating on X-ray emission. In these experiments, RF power was supplied to ECR-II with two power supplies operating at two different frequencies, 14 GHz and 11.1 GHz, while maintaining a constant total power of 300 W. Figure 4 shows the measured total X-ray power and the effective temperature as a function of the fraction of 11.1 GHz power.

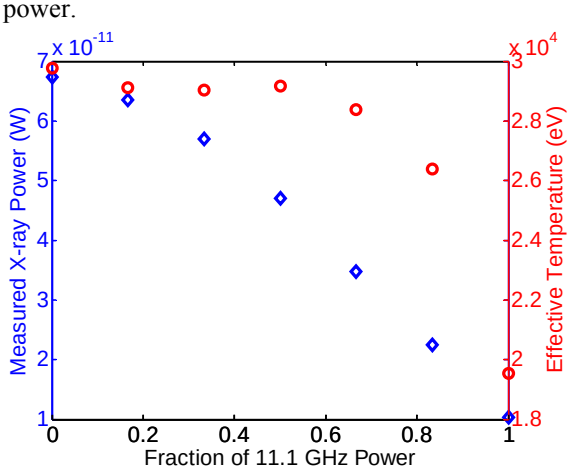

Figure 4: The measured X-ray power over all energies (diamonds) and the effective temperature (circles) vs. the fraction of 11.1 GHz power used.

The total X-ray power decreases by a factor of 7 as the fraction of 11.1 GHz power increases from 0% to 100%. The effective temperature also drops, but only after the 11.1 GHz fraction increases to more than 50%, and only from 30 keV to 20 keV. The corresponding CSDs are shown in Figure 5. A small amount (17%) of 11.1 GHz power pushes the CSD to higher charge states, but further increasing the fraction of lower frequency power causes the CSD to move towards lower charge states. For instance, the current of Ar^{14+} increases by factor of 1.6 as the fraction of 11.1 GHz power increases from 0% to 17%, but then drops by more than an order of magnitude as the fraction increases to 100%.

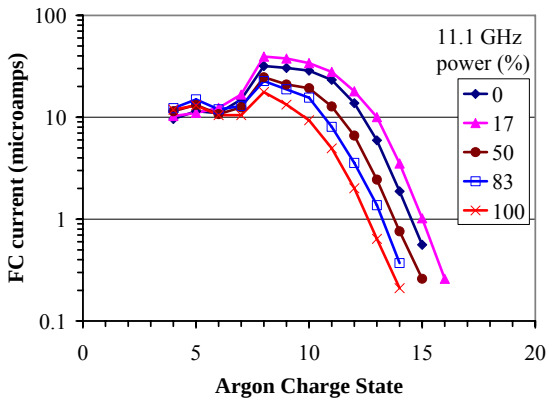

Figure 5: Current to Faraday cup as a function of charge state for different fractions of 11.1 GHz power in the two-frequency heating experiments.

The X-ray signal is also a strong function of the magnetic field strength. Figure 6 shows that both the effective temperature and the total X-ray power increase as the ratio of B_{min} to B_{ECR} increases.

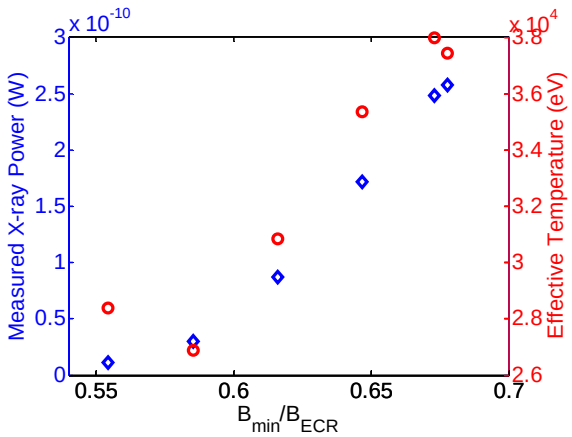

Figure 6: Measured total X-ray power and effective temperature vs. ratio of minimum field to resonance field.

In this experiment, the magnitude of the mirror field was changed while the profile was kept constant by changing the current in the injection and extraction solenoids while keeping the ratio of their currents constant. Since ECR-II has only two solenoid magnets, the ratio of the injection field, B_{inj}, to the extraction field, B_{ext}, and the minimum field, B_{min}, is kept constant. Only one RF power supply was used, at a constant RF frequency of 14 GHz, so that the ratio B_{min}/B_{ECR} is proportional to the strength of the mirror field.

Note the very strong dependence of the measured X-ray power on the strength of the mirror field – a factor of 20 increase for a 20% increase in field strength. The increase in X-ray emission is accompanied by a higher charge states in the CSD, as shown in Figure 7. A 20% increase in magnetic field strength increases the peak of the CSD from Ar^{+8} to Ar^{+10} and gives a factor of 10 increase in the current of Ar^{+14}.

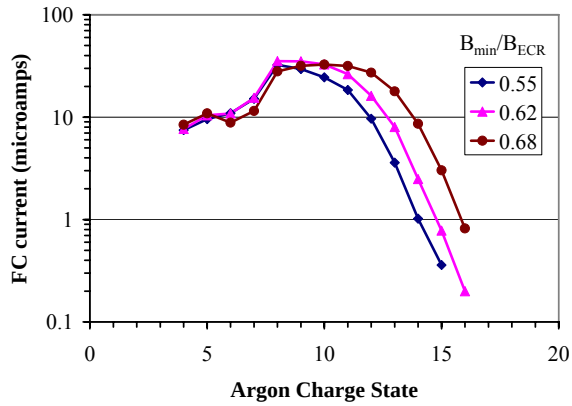

Figure 7: Current to Faraday cup as a function of charge state for different magnetic field strengths.

DISCUSSION

It is clear from the data presented here that much useful information can be obtained by measuring X-ray emission using an inexpensive and robust diode detector. In general, increases in both the intensity and the effective temperature of the X-ray signal tend to be correlated with higher charge states in the CSD. This makes sense, as the same factors that increase X-ray emission (increases in electron density and energy) also lead to higher ionization rates and confinement times.

Many of the experiments presented here have been performed by other researchers, but under different conditions. For instance, previous researchers [8] observed that the intensity of the krypton K_α line decreased with increasing krypton pressure, in apparent contradiction with our results. However, in that experiment the RF power (13 W) was much lower than ours and the gas pressure (>3.8 x 10^{-5} torr) was ~100 times higher. Certainly, the argon $K_{\alpha/\beta}$ line must disappear when the argon pressure goes to zero, as we observed in our experiments. However, we also observed that the intensity of the $K_{\alpha/\beta}$ line started to saturate at higher pressure, and it would not be inconsistent if further increases in the pressure resulted in a drop in the $K_{\alpha/\beta}$ intensity due to a decrease in the electron density and energy.

Increases in X-ray intensity, effective temperature, and charge state with changes in frequency and magnetic field have also been observed by other researchers [9,10], but

the effects are not as dramatic as those we observe. For instance, Figure 4 shows that when using 100% of 11.1 GHz heating then the measured total X-ray power was 1 x 10^{-11} W. At 11.1 GHz, the field strength ratio is B_{min}/B_{ECR} = 0.78. Extrapolating the data in Figure 6 indicates that for 14 GHz heating we would expect to measure around 5 x 10^{-10} W of X-ray power for 14 GHz heating at the same value of B_{min}/B_{ECR}. That is, our results indicate a factor of 50 increase in X-ray power for a factor of 1.26 increase in RF frequency at B_{min}/B_{ECR} = 0.78. This is a remarkable jump in X-ray power, given that theory [11] predicts only a factor of $(1.26)^2$ = 1.59 increase in the electron energy density for this change in RF frequency. In contrast, only a factor of 3 increase in X-ray power for a factor of 1.56 increase in RF frequency at B_{min}/B_{ECR} = 0.70 was reported in [10]. This may be related to the fact that ECR-II uses permanent hexapole magnets, while the data in [10] was obtained from an all superconducting device in which the mirror field and the hexapole field could be scaled together.

Finally, it is interesting to note that while we do observe some increase in the higher charge states, similar to other researchers [12], when employing two-frequency heating with a small amount (17%) of 11.1 GHZ heating, it is not accompanied by an increase in the X-ray power or effective temperature. To our knowledge, the effect of two-frequency heating on the X-ray spectrum has not been systematically investigated by other researchers.

REFERENCES

[1] G. Douysset, H. Khodja, A. Girard, and J. P. Briand, "Highly charged ion densities and ion confinement properties in an electron-cyclotron-resonance ion source," Physical Review E **61**, 3015 (2000)

[2] S. Biri, A. Valek, T. Suta, E. Takacs and Cs. Szabo, L. T. Hudson, B. Radics, J. Imrek, B. Juhasz, and J. Palinkas, "Imaging of ECR plasmas with a pinhole x-ray camera," Rev. Sci. Instrum. **75**, 1420 (2004)

[3] http://www.amptek.com/xr100cdt.html

[4] Schlapp, M. Vondrasek, R.C. Szczech, J. Billquist, P.J. Xie, Z.Q. Harkewicz, R. Pardo, R.C., "A new 14 GHz electron-cyclotron-resonance ion source (ECRIS) for the heavy ion accelerator facility ATLAS," Proc. 1997 Particle Accelerator Conf., 2702 (1997)

[5] L. Schachtera, S. Dobrescu, K. E. Stiebing and J. D. Meyer, "On the physics of metal–dielectric structures in ECR ion sources," Rev. Sci. Instrum. **75**, 1511 (2004)

[6] R. Baskaranb, T. S. Selvakumaran, G. Rodrigues, D. Kanjilal, and A. Roy, "Measurements and analysis of bremsstrahlung x-ray spectrum obtained in NANOGAN electron cyclotron resonance ion source," Rev. Sci. Instrum. **79**, 02A324 (2008)

[7] http://www.amptek.com/anczt1.html

[8] P. Grubling, J. Hollandt, and G. Ulm, "Performance of the new monomode 10 GHz ECR radiation source ELISA," Nuclear Instruments and Methods in Physics Research A **437**, 152 (1999)

[9] T. Nakagawa, Y. Higurashi, M. Kidera, T. Aihara, M. Kase et al., "Effect of magnetic field configuration on the beam intensity from electron cyclotron resonance ion source and RIKEN superconducting electron cyclotron resonance ion source," Rev. Sci. Instrum. **77**, 03A304 (2006)

[10] D. Leitner, J. Y. Benitez, C. M. Lyneis, D. S. Todd, T. Ropponen, J. Ropponen, H. Koivisto, and S. Gammino, "Measurement of the high energy component of the x-ray spectra in the VENUS electron cyclotron resonance ion source," Rev. Sci. Instrum. 79, 033302 (2008)

[11] A Girard, D Hitz, G Melin, and K Serebrennikov, "Electron cyclotron resonance plasmas and electron cyclotron resonance ion sources: Physics and technology," Rev. Sci. Instrum. **75**, 1381 (2004)

[12] R. C. Vondrasek, R. Scott, R. C. Pardo, "ECRIS Operation With Multiple Frequencies," Rev. Sci. Instrum. **77**, 03A337 (2006)